Prediction of Cavitation Erosion in Control Valves Using Computational Fluid Dynamics

Kenji Saito

Chongho Youn

Keywords

Control valve, cavitation erosion, computational fluid dynamics (CFD), visualization, erosion index

Erosion often occurs in control valves due to cavitation. Therefore, for valve manufacturers, the prevention of erosion and suppression of cavitation are important technological problems. As one attempt at a solution, we used an unsteady computational fluid dynamics (CFD) analysis that took cavitation into account, and visualized the results of analysis using published erosion indexes. As a result, we found effective indexes for locations of control valve cavitation erosion, and from the CFD analysis we were able to estimate the relationship between the forms of occurrence of erosion and cavitation.

1. Introduction

A control valve is a device that adjusts the flow of a fluid or stops it completely by moving a plug up and down to control the opening of the flow channel. Control valves are used as final control elements for process control in plants and factory piping systems.

Azbil Corporation produces a large number of valves for specific customers. For example, it has many years of experience in producing high-pressure angle valves for the chemical market and large-diameter control valves for LNG terminals.[1] Given the diverse environments in which they are used, process fluids are subjected to a wide range of conditions. In the case of liquids, cavitation often occurs due to vortexes or the increase of local velocity.

Cavitation refers to a process in which bubbles are formed in a liquid due to a reduction in the liquid's pressure below the saturated vapor pressure, after which the bubbles eventually collapse when the pressure recovers. When these bubbles collapse near a surface, the pressure generated by the collapse is applied to the surface. If this occurs continuously, the surface eventually erodes. Damage to the valve body or inner valve by cavitation erosion can cause serious problems, such as stopping plant production. Against this background, in the past an experiment was conducted on a high-pressure angle valve with a maximum upstream pressure of 20 MPa in order to study cavitation erosion in control valves.[2]

In recent years, on the other hand, erosion indexes calculated by numerical analysis using computational fluid dynamics (CFD) have been proposed as a theoretical method for predicting cavitation erosion, and studies are being conducted on the prediction of erosion locations for objects with blades such as propellers.[3, 4] However, not much study has been done on devices for fluid control, such as control valves, using similar indexes.

In our study, therefore, we analyzed unsteady cavitation using CFD and visualized the results of the analysis using the erosion indexes. In addition, we studied the effectiveness of the erosion indexes and drew inferences about the relationship between erosion that occurs on the plug and the forms of cavitation based on CFD analysis.

Symbols

C_v	:	Flow coefficient
$\dot{m}^+$, $\dot{m}^-$	:	Mass transfer rate
P	:	Pressure
Q	:	Volume flow
α	:	Void fraction
σ	:	Cavitation coefficient
ρ	:	Density

Subscripts

D	:	Downstream
l	:	Liquid phase
U	:	Upstream
v	:	Vapor phase

2. Cavitation Analysis Using CFD

2.1 CFD Model and Analysis Conditions

Figure 1 shows our model of a contoured plug angle valve, which was the subject of the analysis. The valve's shape and dimensions are the same as those of the previously mentioned high-pressure angle valve, and the flow direction is flow-to-open.[2] We extracted the flow channel, which is the computational domain, from figure 1 and generated a mesh. Figure 2 shows the model after mesh generation. The number of elements is approximately 7–8 million. Uniformly distributed static pressure was applied to the inlet and outlet boundaries. The length of the piping in front of and behind the angle valve was 2D on the upstream side and 6D on the downstream side in relation to piping diameter D. The valve travel used in the analysis was 100 % and 90 % of the rated lift.

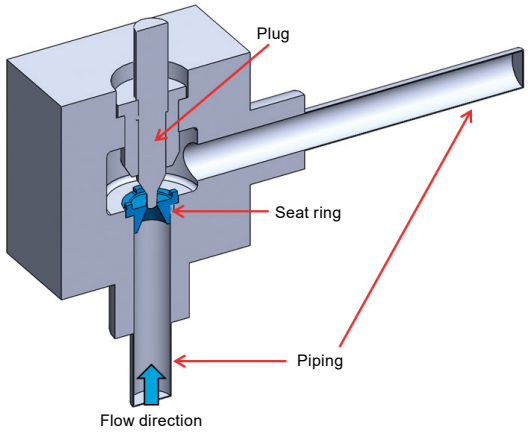

Fig. 1. Cross section of the analyzed model

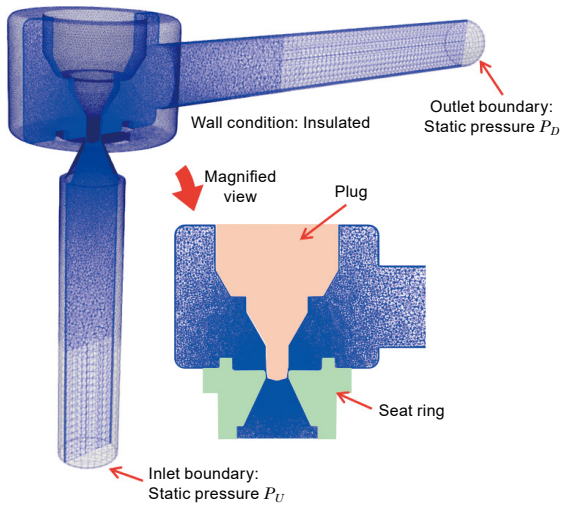

Fig. 2. The model divided into elements

The conditions of the CFD analysis are shown in table 1. Ver. 5.4 of Advance/FrontFlow/red, a general-purpose fluid analysis software, was used as the CFD solver. For the cavitation model, the homogeneous flow model used by Saito et al. was used.[5] In the homogeneous flow model, phase changes during cavitation generation and disappearance are modeled using the following equations:

$$\dot{m} = \begin{cases} \dot{m}^{+} \; if \; P < P_v^* \\ \dot{m}^{-} \; else \end{cases} \tag{1}$$

$$\dot{m}^{+} = C_e A a\,(1-a)\left(\frac{\rho_l}{\rho_v}\right)\frac{P_v^*-P}{\sqrt{2\pi R T_s}} \tag{2}$$

$$\dot{m}^{-} = C_c A a\,(1-a)\,\frac{P_v^*-P}{\sqrt{2\pi R T_s}} \tag{3}$$

$$A = C_a a\,(1-a) \tag{4}$$

In the above equations, T_S is the saturation temperature, P_v* is the saturated vapor pressure, and C_1*=C_eC_a and C_2*=C_cC_a are model constants, each of which is a parameter related to evaporation and condensation rate respectively. In addition, void fraction a is the volumetric fraction of gas in a gas-liquid two-phase flow, and is an important parameter that indicates the amount of bubbles in a certain element.

In a contoured control valve, the separation occurring at the vena contracta causes a large-scale 3D vortex structure and strong swirling flows.[5] Since these are essentially unsteady flows, these strongly unsteady vortex structures cannot be expressed when turbulence motions are modeled using Reynolds-averaged Navier-Stokes equations (RANS) represented by the k-ε model. However, there is a close relationship between how cavitation occurs and vortexes. Therefore, we selected large eddy simulation (LES) as the turbulence model. In LES, only vortexes smaller than the mesh size are modeled, and the motions of vortexes larger than the mesh size are calculated directly. In LES, computation stability is poor and a large-scale computational mesh is required. On the other hand, high-precision results can be expected.

Regarding the wall velocity boundary conditions, normally in LES, non-slip boundaries are set and the resolution of the boundary layer is set high so that the first mesh point is in the viscous sublayer. However, in this study, the model was generated by applying Spalding's law, in view of the broad computational domain and computational cost. Cavitation is repeated rapidly and unsteadily around the plug, which is the focal point of this study. Therefore, the mesh size was set so that the element resolution is highest at the vena contracta and around the plug.

The time step used for computation was fine-tuned to the point at which the cavitation generation and collapse phenomena could be captured. To be specific, it was set so that the Courant number would be at about 10 as the Courant-Friedrichs–Lewy (CFL) condition. As the computational resource, 288 parallel processes were performed using the K computer to reduce the computational time.

Table 1. Computational conditions of CFD analysis

Software	Advance/FrontFlow/red, ver 5.4	
Turbulence model	Large eddy simulation (LES)	
Fluid	Water (25 °C, compressible)	
Mesh cells	100 % opening	6,723,867
	90 % opening	7,899,316
Difference scheme	Momentum	2nd-order upwind
	Energy	1st-order upwind
Wall condition	Spalding's law	
Time step ΔT [s]	2e-06 to 1e-05	
Parallel processes	288	

2.2 Results of Analysis

Validation of the CFD analysis taking cavitation into consideration was conducted first, using the conditions listed in section 2.1. The conditions of analysis are shown in table 2. Here the cavitation number σ is defined by equation (5):

$$\sigma = \frac{P_U - P_v^*}{P_U - P_D} \tag{5}$$

CFD analysis was conducted under the conditions listed in table 2, and the flow coefficient C_v was calculated from the obtained flow rate. It is shown in figure 3, along with the flow coefficient of the result of the above-mentioned past experiment conducted under the same conditions as those in table 2.[2] Comparison of the flow coefficients of the CFD analysis and the prior experiment reveals an error of approximately 2 %, showing that the two are in close agreement.

Table 2. Test conditions

Cavitation number σ	1.13
Lift [%]	100
Upstream pressure P_U [kPa (abs)]	1,100
Downstream pressure P_D [kPa (abs)]	128.7

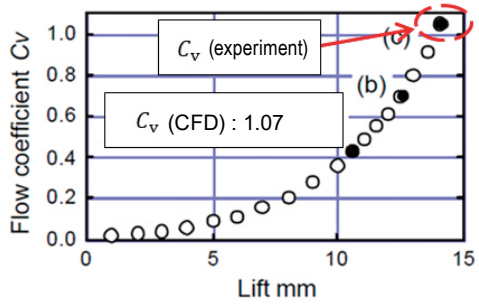

Fig. 3. Flow coefficients obtained by experiment[2] and by CFD analysis

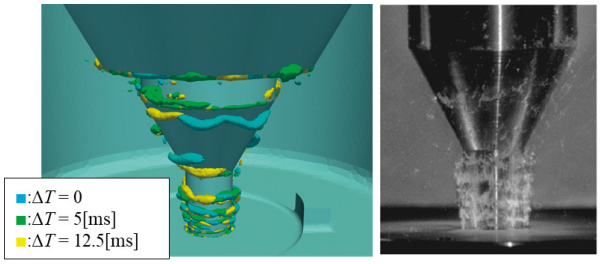

Isosurface with a void fraction of 0.05 obtained from CFD analysis

Photograph[2] under the same conditions as those of the CFD analysis

Fig. 4. Comparison of CFD analysis (void fraction α = 0.05) and experiment

Figure 4 shows a contour plot with void fraction α = 0.05 and a photograph of the moment at which bubbles were generated in the experiment. From this figure, a qualitatively reasonable result was obtained concerning the occurrence conditions of bubbles.

From the above results, the CFD analysis model used in this study is believed to be valid.

3. Numerical Analysis of Cavitation Erosion

3.1 Erosion Indexes

Erosion indexes express the intensity of erosion as functions, assuming that changes in bubbles or pressure on the surface of an object are parameters that define the erosion's intensity. In this study, the following equations proposed by Nohmi et al.[4] were used as erosion indexes:

$$\text{Index 1: } \frac{1}{T_c}\int_0^{T_c} a \cdot max\left[\frac{\partial P}{\partial t}, 0\right] dt \tag{6}$$

$$\text{Index 2: } \frac{1}{T_c}\int_0^{T_c} a \cdot max\left[P - P_v^*, 0\right] dt \tag{7}$$

$$\text{Index 3: } \frac{1}{T_c}\int_0^{T_c} max\left[-\frac{\partial a}{\partial t}, 0\right] dt \tag{8}$$

$$\text{Index 4: } \frac{1}{T_c}\int_0^{T_c} max\left[P - P_v^*, 0\right] \cdot max\left[-\frac{\partial a}{\partial t}, 0\right] dt \tag{9}$$

In the above indexes, Tc is the period of cavitation occurrence, and the one-period time integration was used in this study. In section 3.2, the results of CFD analysis were visualized and evaluated using the indexes of equations (6) to (9).

3.2 Comparison with Experimental Erosion Results

In order to examine the validity of the erosion indexes shown in section 3.1, each index was compared with the experimental results. The CFD analysis conditions and experiment conditions are shown in table 3. There were two cases, Case 1 and Case 2, with differing downstream pressures. The plug photos in the experimental results were taken after 30 hours had elapsed. The plug material is SUS316.

In figures 5 and 6, contour plots of the results of analysis using the erosion indexes of equations (6) to (9) and the results of the erosion that occurred at the plug during the experiment are shown. Comparison of the two cases of erosion in the experiment shows that erosion occurred on the plug seat surface, conical surface, and the end of the conical surface, but it occurred differently in Case 1 and Case 2. From the contour plots for Case 1, it can be observed that Index 3 shows a high value at the plug tip, which does not agree qualitatively with the result of the experiment. Index 1, Index 2, and Index 4 show conditions similar to those of the experimental results.

Table 3. Erosion experiment conditions

Experimental conditions	Case 1	Case 2
Cavitation number σ	1.058	1.041
Lift [%]	90	
Upstream pressure P_U [MPa (abs)]	20	20
Downstream pressure P_D [MPa (abs)]	1	0.8

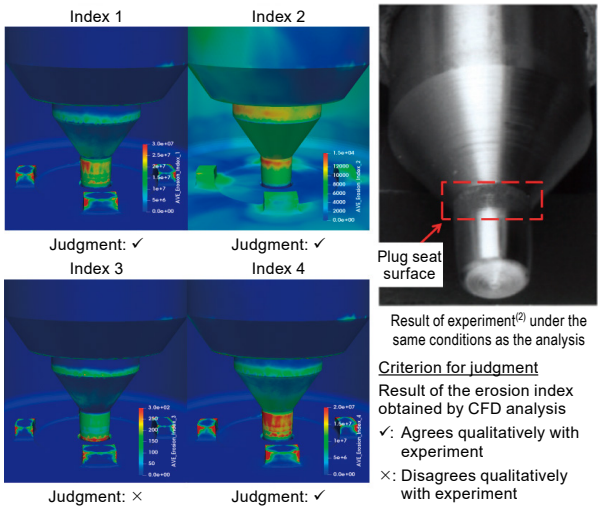

Fig. 5. Erosion indexes and plug erosion (Case 1)

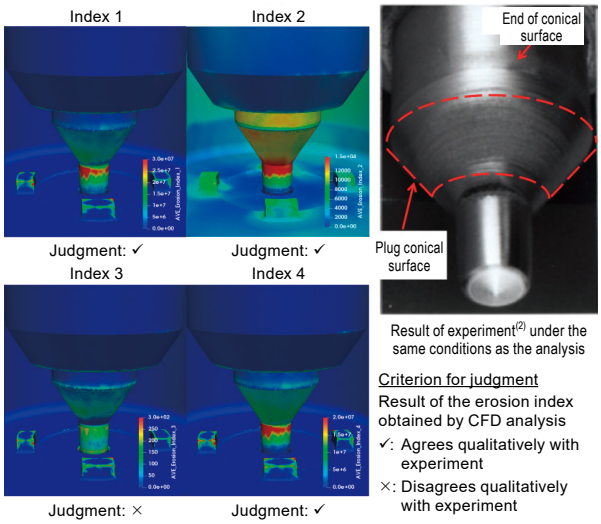

Fig. 6. Erosion indexes and plug erosion (Case 2)

In Case 2, it is clear from the photos of the experimental results that erosion also occurred across the plug conical surface, in addition to the seat surface. Although Index 3 did not agree with the experimental result in Case 2 either, Indexes 1, 2, and 4 did not show much difference from the experimental result.

From the above results, erosion indexes 1, 2, and 4 are believed to be effective for identifying locations with erosion risk.

3.3 Erosion by Cavitation Flow

In this section, based on the results of CFD analysis of unsteady cavitation flow, we will examine the reason why cavitation erosion differed in Case 1 and Case 2, as was described in section 3.2. For both Case 1 and Case 2, a sufficiently time-evolved flow field was formed, and then changes in the cavitation flow after time ΔT had elapsed were visualized and evaluated. The cross-section for analysis and evaluation is shown in figure 7(a), and the contour plots of the visualized void fractions are shown in figure 7(b).

As shown in figure 7, bubbles are generated near the vena contracta of the plug both in Case 1 and Case 2, and the generated bubbles move from the front of the plug toward the seat surface along with the flow. These bubbles are thought to be cavitation generated by vortexes detached from the plug and seat ring.

The result at ΔT = 1 [ms] for Case 1 shows that the bubbles collapse near the seat surface before reaching the conical surface of the plug. It is assumed that, under the conditions for Case 1, this bubble collapse continually occurred and caused erosion only near the seat surface.

In Case 2, it was observed that the portion of the plug that determines flow characteristics was covered by a layer of bubbles. This is believed to have been caused by the development of sheet cavitation. From studies on bladed objects, it is known that, after sheet cavitation develops with time, a portion of bubbles separates from it and flows downstream as a cloud-like lump (cloud cavitation).[6] The results of Case 2 show that sheet cavitation changed to cloud cavitation, collided with the conical surface, and then collapsed. In addition, since cloud cavitation is a major cause of cavitation erosion, it is believed that in Case 2 erosion occurred when bubbles that had separated from the plug surface collided with the plug conical surface and then collapsed.

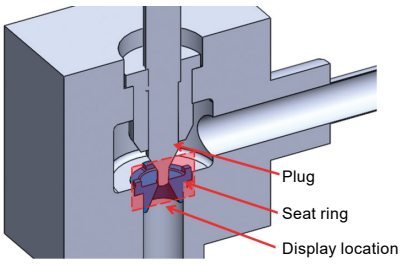

7(a) Cross-section for analysis and evaluation

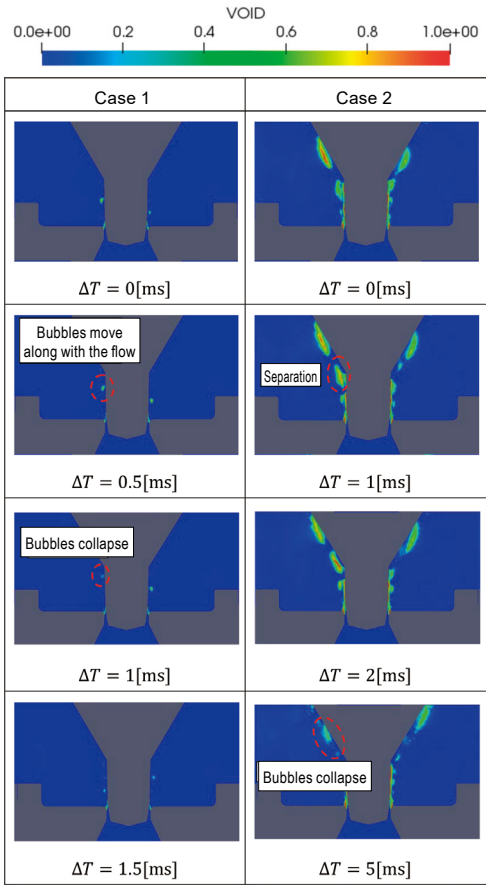

7(b) Changes in the cavitation flow

Fig. 7. Cavitation in Cases 1 and 2

From the above CFD analysis results, the difference between the cavitation erosion in Case 1 and Case 2 is believed to be due to a difference in the form of cavitation.

4. Conclusion

In this study, a CFD analysis was conducted to examine cavitation in angle control valves, and erosion indexes thought to be effective in the prediction of cavitation erosion in control valves were compared.

As a result of an analysis of unsteady cavitation conducted using LES as the turbulence model, the following results were obtained:

(1) As a result of evaluation of erosion using the erosion indexes, erosion indexes 1, 2, and 4 were effective in identifying locations with erosion risk.

(2) Differences in the cavitation erosion that occurred on the plug surface are believed to be due to different forms of cavitation.

In the future, it is necessary to establish a method of evaluating erosion using CFD analysis by quantitatively evaluating the amount of cavitation erosion that occurs in experiments and the values of erosion indexes. If it becomes possible to predict cavitation erosion in the design and development phase, the performance and quality of control valves will be significantly improved, which will contribute to the long-term safe operation of plants and the development of basic industries.

References

(1) K. Nakahashi. “Characteristics of automatic control valves for low-temperature applications and their practical design” (in Japanese). *Valve Technical Review*, Vol. 20, No. 1319, 1991, pp. 32–41.

(2) S. Yuzawa. “Cavitation and erosion in control valves by pressure reduction and flow regulation of high-pressure liquid” (in Japanese). Doctoral dissertation, Waseda University, 2003.

(3) O. Usta, B. Aktas, M. Maasch, O. Turan, M. Atlar, and E. Korkut. “A study on the numerical prediction of cavitation erosion for propellers.” *Proceedings of the Fifth International Symposium on Marine Propulsors* (Finland, 2017).
Available at http://www.marinepropulsors.com/proceedings-2017.php.

(4) N. Hasuike, S.Yamasaki, J. Ando, and A. Okazaki. “Numerical study on cavitation erosion risk of marine propellers operating in wake flow.” *Journal of the JIME*, Vol. 46, No. 3, 2011, pp. 79–87 (alternate pagination pp. 366–374).

(5) Y. Saito, I. Nakamori, and T. Ikohagi. “Numerical analysis of unsteady vaporous cavitating flow around a hydrofoil.” Fifth International Symposium on Cavitation (CAV2003), Osaka, Japan, 2003.
Available at http://flow.me.es.osaka-u.ac.jp/cav2003/Papers/Cav03-OS-1-006.pdf.

(6) Y. Kato (ed.). *Cavitation: Fundamentals and Recent Advances* (in Japanese). New edition. Morikita Publishing Co., Ltd., 2016, pp. 124–27.

Authors

Kenji Saito, Valve Product Development Department, Azbil Corporation

Chongho Youn, Valve Product Development Department, Azbil Corporation